SERI/STR-211-3448
DE89000890

March 1989

Investigations of the Origins of Metastable, Light-Induced Changes in Hydrogenated Amorphous Silicon

Final Subcontract Report
1 February 1986 - 30 March 1988

J. D. Cohen
Department of Physics
University of Oregon
Eugene, Oregon

Prepared under Subcontract No. XB-6-06024-1

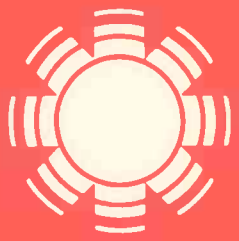

SERI

Solar Energy Research Institute
A Division of Midwest Research Institute

1617 Cole Boulevard
Golden, Colorado 80401

Operated for the
U.S. Department of Energy
under Contract No. EG-77-C-01-4042

SERI/STR-211-3448
UC Category: 271
DE89000890

SERI/STR--211-3448

DE89 000890

Investigations of the Origins of Metastable, Light-Induced Changes in Hydrogenated Amorphous Silicon

Final Subcontract Report
1 February 1986 - 30 March 1988

J. D. Cohen
Department of Physics
University of Oregon
Eugene, Oregon

March 1989

SERI Technical Monitor: B. Stafford

Prepared under Subcontract No. XB-6-06024-1

Solar Energy Research Institute
A Division of Midwest Research Institute

1617 Cole Boulevard
Golden, Colorado 80401-3393

Prepared for the
U.S. Department of Energy
Contract No. DE-AC02-83CH10093

NOTICE

Printed in the United States of America
Available from:
National Technical Information Service
U.S. Department of Commerce
5285 Port Royal Road
Springfield, VA 22161

Price: Microfiche A01
Printed Copy A03

Codes are used for pricing all publications. The code is determined by the number of pages in the publication. Information pertaining to the pricing codes can be found in the current issue of the following publications which are generally available in most libraries: *Energy Research Abstracts (ERA)*; *Government Reports Announcements* and Index (*GRA* and I); *Scientific and Technical Abstract Reports (STAR)*; and publication NTIS-PR-360 available from NTIS at the above address.

TABLE OF CONTENTS

LIST OF ILLUSTRATIONS

LIST OF TABLES

page

EXECUTIVE SUMMARY

We have developed and exploited two types of junction capacitance methods for the study of metastable effects in a-Si:H films. First of all, using the drive-level capacitance profiling method, we have extended our studies comparing the density of light-induced metastable defects to two new "totally phosphorous free" samples. We also began to better exploit the profiling aspect of this technique by comparing the spatial dependence of the metastable deep state distribution with the SIMS determined impurity profiles for these samples. Such studies reinforce earlier conclusions that there exists a strong correlation of the impurity content in a-Si:H films with the degree of the light-induced defect creation, particularly in the case of carbon impurities. Second, we developed the method of transient photocapacitance spectroscopy to the study of undoped films. By comparing such spectra to junction transient photocurrent spectra taken under identical conditions, we found we could unambiguously separate the electron and hole emission transitions from deep gap states. Our analysis also allowed us to determine the hole products. By comparing films before and after light soaking we found that the $(\mu\tau)_h$ product was substantially larger for the light-induced defects than for the intrinsic defects. Finally, we applied both the drive-level capacitance profiling method and the transient photocapacitance method to the study of metastable effects in n-type doped samples. The results of these studies were utilized to distinguish among various proposed defect reactions which might be responsible for the observed changes in Fermi level position, occupied bandtail states, and density of deep "dangling bond" defects. Our results indicate, however, that none of the suggested reactions could explain the behavior of the most lightly doped samples and indicate, instead, that there exists a reaction involving dopant vs. non-doping configurations of P by itself.

1.0 INTRODUCTION

The focus of the research program supported under our SERI subcontract is the investigation of metastable defect creation processes in hydrogenated amorphous silicon (a-Si:H). To carry out this investigation we primarily rely on junction capacitance methods to monitor the changes in the deep defect distribution. These methods have allowed us to test different aspects of such metastable effects than those disclosed by such techniques as electron spin resonance (ESR) [1,2], photoconductivity [3,4], or optical absorption techniques [5]. Particular advantages of the junction capacitance techniques are the ability to spatially profile defects within a single sample, to separate hole from electron gap state processes, and to determine absolute levels of defect densities.

This report, which covers Phase II of our just concluded two year funding period, will cover three specific areas of study. First, we will briefly summarize results obtained to date employing our capacitance profiling methods to the study of undoped samples which indicate a significant role for extrinsic impurities in the degree of light induced degradation. This conclusion has recently been strengthened regarding the role of carbon impurities by a direct comparison in one sample of the SIMS determined impurity profiles with the capacitance profile of the light induced defects.

Second, we will report significant progress on our studies utilizing photocapacitance transient measurements to investigate metastable changes in undoped a-Si:H. In these studies we compare the transient photocapacitance with the photocurrent transient spectra at different temperatures and different degrees of light soaking. In the last year, by successfully modelling such spectra, we have been able to unambiguously separate the optical transitions originating from the valence and conduction bands and, in addition, to identify both the increase in the deep defect densities plus the degradation in the hole mobilities which result from light soaking. These result indicate a significant increase in the hole capture rate of the light-induced defects as compared to the intrinsic deep defects.

Finally, in Phase II of this funding period we have also begun some studies of the metastable changes in n-type doped a-Si:H samples using both the drive-level capacitance profiling technique and the transient photocapacitance methods which we have been utilizing in our studies of undoped films. Preliminary results on three samples with different doping levels indicate (1) a significantly different energy distribution for the deep defects depending on the degree of partial annealing from the light soaked state; and (2) a clear indication of two distinct regimes of metastable effects. The first regime seems to specifically involve a change in the deep defect density whereas the second (observed during the higher temperature range of partial dark anneals) is characterized by a Fermi level shift and

change in occupied conduction bandtail states but without any discernable change in the density of deep states.

In the final section of this report we will summarize what has been learned about the detailed mechanisms of metastable changes in a-Si:H based on this work. We will also comment on which specific issues are most likely to merit further investigation.

2.0 SAMPLES AND SAMPLE TREATMENT

2.1 GROWTH PARAMETERS OF UNDOPED SAMPLES

The undoped samples used in these studies have been described in some detail in last year's annual report. These 8 samples were produced by the glow discharge method using substrate temperatures of 255 ± 5 ^{o}C. The SiH_4/Ar dilution for each of the samples are listed in Table I along with the impurity levels determined by SIMS analysis [6]. The phosphorous level for sample 1 was found to be sufficiently high that this sample must be considered n-type (this one sample was produced on a different growth system than the other 7 samples). For the remaining samples the phosphorous level is seen to amount to a few ppm or less. In particular, samples 7 and 8 were grown after a complete etching of the growth chamber followed by a 6 hour deposition of SiH_4 to coat the chamber walls before actual sample deposition. The undetectable level of phosphorous for sample 7 (of less than 5×10^{15} cm^{-3}) determined by SIMS verifies that this sample was, indeed, found to be essentially phosphorous free. We believe that sample 8, grown immediate subsequent to sample 7, is equally phosphorous free (the 0.2 ppm phosphorous level indicated by SIMS for this sample was more likely due to partially hydrogenated ^{28}Si or ^{29}Si radicals instead of ^{31}P).

2.2 GROWTH PARAMETERS OF N-TYPE DOPED SAMPLES

Because of an long history of research in our laboratory of the fundamental processes in doped a-Si:H films, an extensive series of PH_3-doped n-type a-Si:H films are available for study. For a preliminary study of metastable effects in such films using our recently developed techniques, we chose 3 of these films which had been grown at a 40% SiH_4 dilution level in Ar within the last year with doping levels of 30 vppm, 100 vppm, and 300 vppm PH_3, respectively. The rf power levels and substrate temperatures were identical to those of our undoped samples.

2.3 PREPARATION OF METASTABLE STATES OF SAMPLES

For all results reported below the "dark annealed state" (state A) refers to a sample which has been heated in the dark at 45 minutes at 200^{o}C and then cooled in the dark at a rate of roughly 5^{o}C/second. The "light saturated state" (state B) was

reached by exposing the film to 1.9 eV light from a cw krypton laser at 400mW/cm^2 (corrected for the semitransparant metal contact) at room temperature for 2.5 hours. Partially annealed "states" were obtained by typically 15 minute isochronal anneals. For our studies of undoped samples we began at 380K (state B1) and progressed at 10 to 30K intervals to 470K. In general, because our capacitance measurements in undoped samples are usually carried out at somewhat elevated temperatures (360-400K), data for the most light soaked state is usually given beginning with state B1 or B2 (the state obtained after the second partial anneal typically at 400K or 410K) to minimize possible annealing during the period in which the spectra are compiled.

For our n-type doped samples the initial anneal state (B1) denotes a 350K anneal and subsequent anneals proceeded at 30K intervals up to 470K.

3.0 DESCRIPTION OF EXPERIMENTAL TECHNIQUES

3.1 DRIVE-LEVEL CAPACITANCE PROFILING

The drive-level capacitance profiling technique was developed in 1984-85 in our laboratory and has been described in several publications [7,8] and in our previous SERI Annual Reports for 1985, 1986, and 1987. For completeness only, we will briefly summarize a few of the important features of this method.

Capacitance-voltage (CV) profiling is a standard technique in the characterization of semiconductors which allows one to map out the doping level of a sample versus distance, typically over several tenths of a micron. Unfortunately, due to the high concentration of deep defects over a significant fraction of the gap in a-Si:H, this method fails to be easily interpretable for this material. To overcome this limitation and be able to similarly obtain spatial profiles of gap states in a-Si:H, we developed an alternative technique which examines in detail the dependence of the junction capacitance as a function of applied bias, temperature, plus the peak-to-peak drive amplitude of the alternating component of the junction voltage, dV. In general, one finds that the measured ac capacitance at a particular DC bias depends on dV according to the relation

$$C = C_0 + C_1\, dV + C_2\, (dV)^2 + \ldots \qquad (1)$$

One can experimentally determine the coefficients C_0 and C_1. We have shown that a simple algebraic expression using these coefficients then directly yields an integral over the density of gap states [7]:

$$N_{DL} = \frac{-C_0^3}{2\epsilon q A^2 C_1} = \int_{E_c - E_e}^{E_F^o} g(E)\, dE \qquad (2)$$

where ϵ is the dielectric constant, A is the junction area, E_F^o is the Fermi level position in the neutral bulk a-Si:H, E_c is the bottom of the conduction band (mobility) edge, and E_e is determined by the temperature, T, and (angular) frequency ω of the capacitance measurement, namely

$$E_e(T,\omega) = k_B\, T \log(\nu/\omega). \qquad (3)$$

Hence one experimentally obtains an integral over the density of gap states and can spatially profile this energy "slice" of deep defects by varying the DC applied bias as in conventional CV profiling and plotting the drive-level density, N_{DL}, versus $\epsilon C_0/A$. By repeating such profiles at different temperatures one can vary the energy range of the integral and thus obtain g(E) itself. Indeed, we believe that the drive-level profiling technique represents the most reliable method to separately map out both the spatial and energy variation of the defect density in amorphous silicon films. Examples of data obtained by this technique are presented in Section 4.

3.2 JUNCTION TRANSIENT PHOTOCAPACITANCE SPECTROSCOPY

Because the drive-level method only allows us to examine g(E) over a fairly restrictive energy range, particularly for undoped samples (between roughly 0.75 to 0.95 eV below E_c) we have, during this Subcontract period, begun to employ photocapacitance transient spectroscopy to the study of metastable effects in a-Si:H films. The transient photocapacitance technique we use was first developed to study optical processes in doped a-Si:H [9]. In general, such photocapacitance spectra appear qualitatively quite similar to sub-band-gap optical absorption spectra (see Fig. 2 as well as spectra displayed in Sections 5 and 6). However, there are several important differences. Most significant, perhaps, is that photocapacitance detects the net charge change in the depletion region of the sample. Hence, hole and electron transitions from gap states give signals of opposite sign. Second, because photocapacitance generally detects transitions in the depletion width, one can vary the spatial region be examined by varying the DC bias as with other junction capacitance methods. Third, this technique is typically 10^2-10^3 times more sensitive than photo-thermal spectroscopy (PDS) optical absorption techniques [5]. This is due to the fact that charge detection is intrinsically a very sensitive measurement. Finally, it is straightforward to vary the measurement temperature over a wide range and thus observe competition between the optical and thermal excitation processes.

Like optical absorption measurements, photocapacitance is relatively straightforward to interpret since it is not greatly affected by the details of the transport processes provided that measurement time scales are long compared to both dielectric relaxation times and carrier transit times across the depletion region. For our undoped samples we employ a 100 Hz voltage source and record transients on a time scale of several seconds. We also operate at somewhat elevated temperatures (340-390K) to ensure that dielectric relaxation times will be sufficiently short. For the studies of doped samples such concerns are rarely a problem and we typically operate at 10 kHz because of the improved signal to noise one obtains in capacitance measurements at higher frequencies.

The time sequence of these experiments is illustrated in Fig. 1. A voltage pulse is used to fill gap states with electrons in the depletion region of the sample. Sub-bandgap light of a chosen optical energy is introduced after the voltage pulse to assist the re-equilibration of trapped carriers. However, we record every second transient without this sub-bandgap light so that a dark transient baseline can be established. The photocapacitance transient for optical energy E_{opt}, $C(E_{opt},t)$, is the <u>difference</u> between the transients recorded in the light and dark. This transient is processed by multiplying it by a correlator function, $F_c(t)$, and integrating over a time window following each voltage pulse:

$$S(E_{opt}) = \int_{t_i}^{t_f} F_c(t)\ C(E_{opt},t)\ dt \qquad (4)$$

The photocapacitance <u>spectrum</u> is obtained by plotting the resultant, intensity normalized signal versus optical energy at constant temperature. Particular care is taken to operate at sufficiently low light levels that strict linearity to intensity is observed. In Fig. 2 we give several examples of photocapacitance spectra for both doped and undoped samples. For the doped sample we show spectra taken at two very different temperatures. At low temperatures for doped samples we see that it is possible to obtain high quality spectra to optical energies below 0.5 eV using a tungsten-halogen light source. The spectrum for this sample shown at high temperature indicates that the general appearance of such spectra, which reflects the position of the dominant deep defect band, is indeed fairly temperature independent. We also note the general qualitative similarity of the spectra for both n-type doped and intrinsic samples.

As a rule, we record the transient junction (primary) photocurrent spectra in exactly the same manner. These spectra give us a useful point of reference for comparison to other studies. More importantly, these photocurrent spectra provide very important supplemental information, as we discuss in Sections 5.1 and 5.2 below.

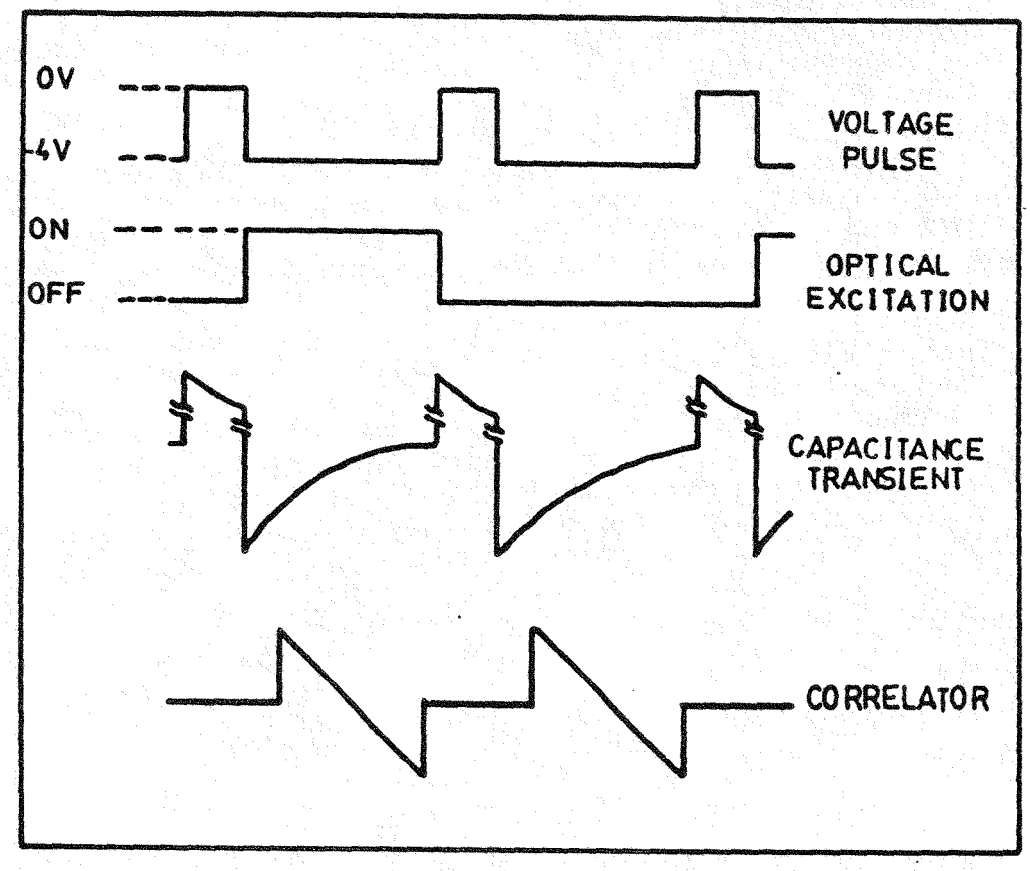

FIG. 1. Schematic of photocapacitance measurement technique. Shown are the time sequence of the applied sample voltage, the exposure to sub-bandgap light, the capacitance transient signal, and the correlator function used to process the transient signal.

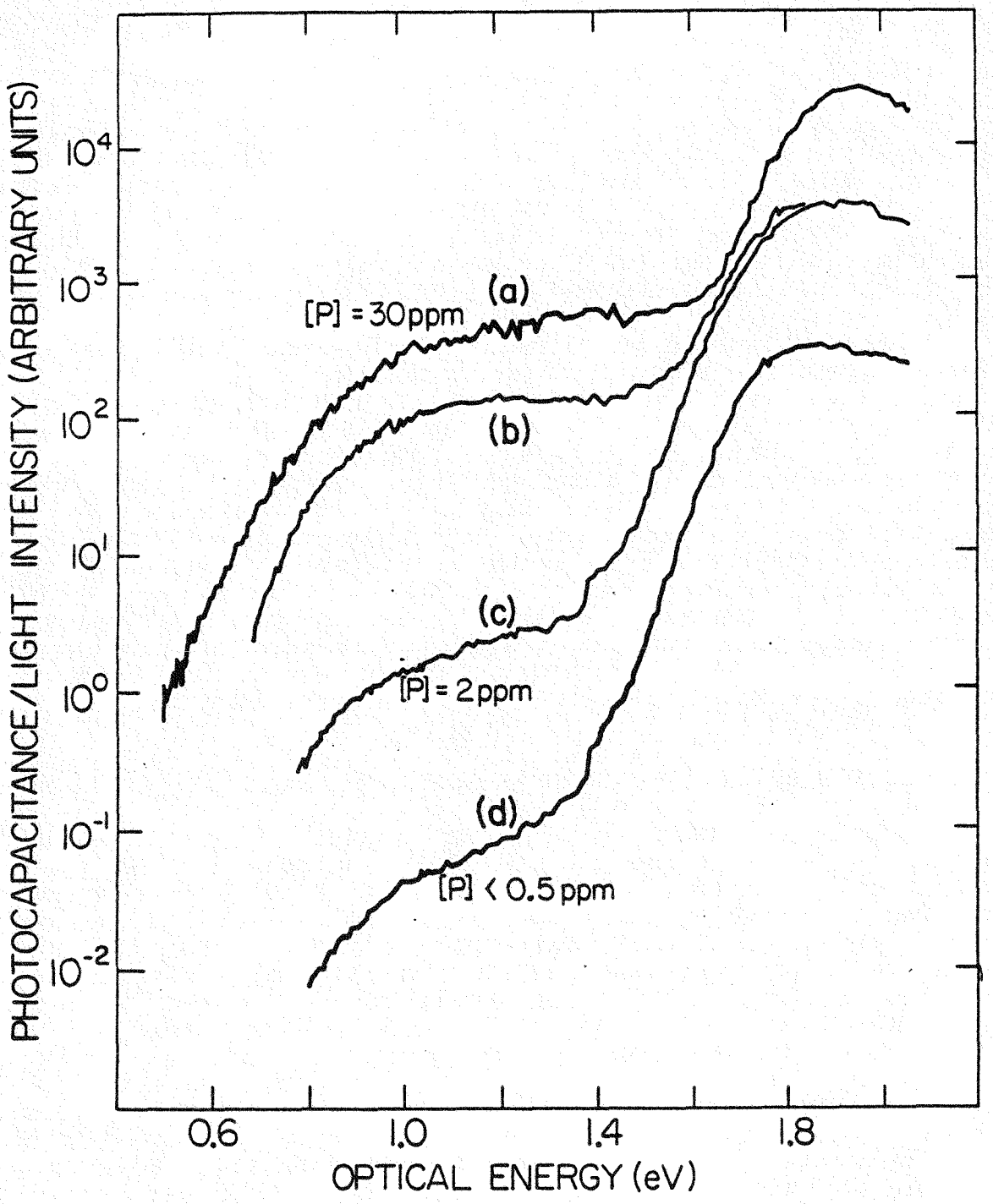

FIG. 2. Examples of transient photocapacitance spectra for a-Si:H samples with different doping levels. Spectra (a) and (b) were taken on a 30 vppm PH_3 sample at a 100 Hz measurement frequency and temperatures of 140 K and 360 K, respectively. Spectra (c) and (d) were taken at 100 Hz and 380 K for two samples with SIMS determined phosphorous levels of 2 ppm and less than 0.5 ppm, respectively.

4.0 ROLE OF EXTRINSIC IMPURITIES ON STABILITY IN UNDOPED FILMS

4.1 SUMMARY OF DRIVE-LEVEL RESULTS VS. IMPURITY CONTENT

We have discussed our drive-level profiling results on undoped samples in quite some detail in previous reports [8]. However, full SIMS results on our most recent "totally phosphorous free" samples were only obtained during the current year [6]. Thus we present in Table I a full summary of the SIMS results for all 8 samples studied in this manner along with the deep defect densities deduced for states A and B1.

We have attempted to correlate light induced changes in deep defects (i.e., the state B1 density minus that in state A) among these samples with the difference in the atmospheric impurity content. We note that while samples 4, 5, and 6 have comparably low defect densities in state A, the metastable defect density of these samples varies by a factor of 6, roughly in proportion to their carbon content. Both samples 7 and 8 also show quite a large increase in defects after light exposure and this behavior does appear to show some correlation to the somewhat higher oxygen levels in these samples. An active role for oxygen in the stability of a-Si:H has previously been suggested [10]; however, in our samples this conclusion seems to be at odds with one other study which indicates no oxygen related extrinsic component to the Staebler-Wronski effect until somewhat higher levels of oxygen are reached [2].

4.2 PROFILES OF LIGHT-INDUCED DEFECTS VS. IMPURITY PROFILES

The fairly strong evidence of a carbon related extrinsic component to the degree of stability in some a-Si:H has been tested further in one film (sample 4). This particular sample exhibited a fairly distinctive spatial dependence of its carbon impurity level which was considerably different than the spatial dependence of the oxygen and nitrogen levels. Because of the profiling ability of our measurements we decided to try to compare the spatial dependence of deep defects before and after light exposure to the SIMS impurity profiles directly. This kind of comparison is shown in Fig. 3. The two defect profiles displayed (for state A and state B2) cover slightly different spatial regions due to the different extent of the depletion region depending on the number of deep defects. However, the change in distribution of deep defects is quite clear: in state A this distribution is essentially spatially uniform, while for state B2 there is marked spatial dependence of deep defects which matches quite closely that of the carbon profile in this sample. Hence, we believe, the evidence for an extrinsic carbon component to instability in this sample is quite compelling.

TABLE I. Results of SIMS impurity analysis of the six glow discharge produced films along with deep defect concentration in state A and state B1 determined by drive-level capacitance profiling. Impurity concentrations are given in the spatial region examined by the capacitance profiling.

Sample	SiH_4/Ar Ratio (%)	Impurity Concentrations				Deep Defect Density	
		Phosphorous (cm^{-3})	Oxygen (cm^{-3})	Nitrogen (cm^{-3})	Carbon (cm^{-3})	State A (cm^{-3})	State B1 (cm^{-3})
1	50	2×10^{18}	4×10^{19}	1×10^{18}	3×10^{18}	2.4×10^{16}	5.3×10^{16}
2	30	7×10^{16}	2×10^{19}	* 4×10^{18}	3×10^{18}	3.1×10^{16}	7.2×10^{16}
3	100	8×10^{16}	2.5×10^{19}	*1.5×10^{19}	*2.5×10^{18}	2.4×10^{16}	4.3×10^{16}
4	30	* 1×10^{17}	3×10^{19}	2.5×10^{18}	* 7×10^{18}	4.9×10^{15}	1.7×10^{16}
5	10	2×10^{16}	1.5×10^{19}	1.5×10^{18}	3×10^{18}	3.5×10^{15}	8.6×10^{15}
6	100	6×10^{16}	2×10^{19}	2×10^{18}	*1.4×10^{19}	4.4×10^{15}	3.6×10^{16}
7	50	$< 5 \times 10^{15}$	5×10^{19}	1.5×10^{18}	1.4×10^{18}	4.4×10^{15}	2.4×10^{16}
8	100	* 1×10^{16}	7×10^{19}	2×10^{18}	2×10^{18}	3.2×10^{15}	3.2×10^{16}

* SIMS analysis indicated a spatial variation for this impurity in excess of a factor of 1.5/μm.

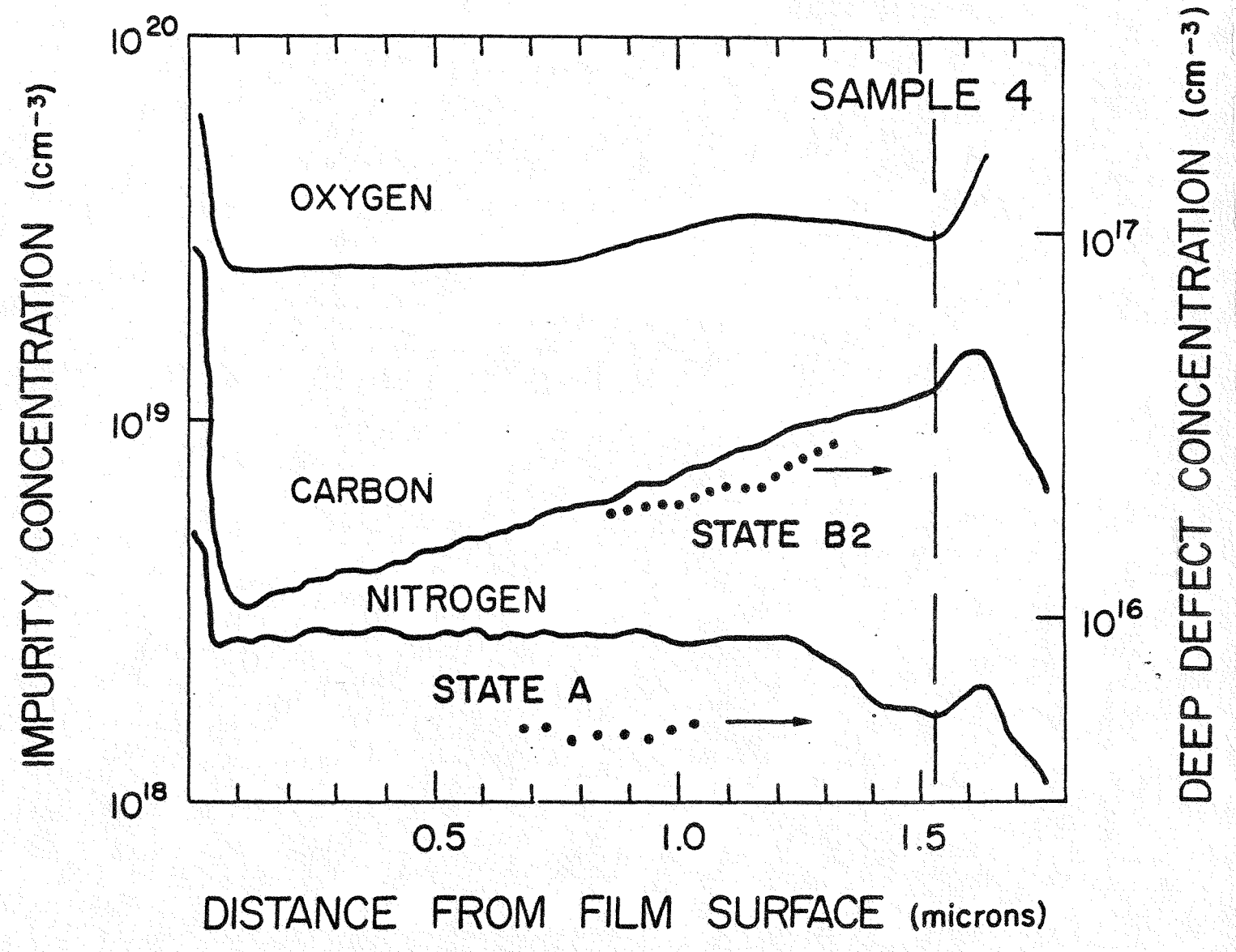

FIG. 3. Comparison of SIMS impurity level profiles with light-induced metastable defect profile. The levels of the oxygen, carbon, and nitrogen impurities are indicated on the left scale while the drive-level profiles for midgap defect densities in State A and B are indicated on the right hand scale. Note the strong similarity between the carbon profile and the metastable deep defect density.

5.0 TRANSIENT PHOTOCAPACITANCE STUDIES OF METASTABLE EFFECTS IN UNDOPED FILMS

5.1 COMPARISON OF PHOTOCAPACITANCE AND PHOTOCURRENT SPECTRA

Transient photocapacitance and photocurrent spectra for sample 5 taken at two different temperatures are shown in Fig. 4. To compare these spectra we have chosen to overlap the two kinds of spectra at each temperature in the energy regime below 0.9 eV. We believe this is the regime where both kinds of measurements should respond to gap state transitions in the same manner since, for energies below midgap, the only excitation possible will be an electron from a trapped gap state to the conduction band. At a 1.2 eV excitation energy, on the other hand, several kinds of transitions are possible. Possible candidates are (see Fig. 5):

(a) $D^- \longrightarrow D^o + e$ (b) $D^o \longrightarrow D^+ + e$ (c) $D^o \longrightarrow D^- + h$

where D^-, D^o, and D^+ denote the 3 charge states of the dominant deep defect. In a photocurrent measurement both (a) and (c) will give <u>additive</u> signals while in a photocapacitance measurement they will correspond to opposite changes in depletion and thus be <u>subtractive</u> (this will, of course, also depend on the ability of the emitted hole to leave the depletion region). Likewise the signals from transitions of type (b) can also be different: If the D^+ can thermally emit a hole on a time scale that is fast compared to our measurement time it will become a D^o again and thus negate the change in the depletion region charge from the photoexcited electron and yield an overall null photocapacitance signal. However, such a process will actually enhance the transient photocurrent signal.

Similarly, transitions from the valence bandtail (VB-tail) to the conduction band should give a positive contribution in photocapacitance due to the removal of one gap state electron; however, the remaining VB-tail hole will undergo rapid thermal emission to the valence band where, depending on the hole mobility, it may leave the depletion region. If it escapes, the overall change in photocapacitance will be small. Again, the transient photocurrent signal will be enhanced.

More accurately, if A electrons and B holes leave the depletion region during the measurement time window, the total transient photocurrent signal will roughly be proportional to $A + (1/2)B$ while the total transient photocapacitance signal will be proportional to $A - B$. The coefficient of 1/2 for hole processes in the transient photocurrent signal is related to the different spatial sensitivity for majority and minority carrier emission of the junction photocurrent [11]. (The capacitance signal has identical spatial sensitivity for both types of emission.)

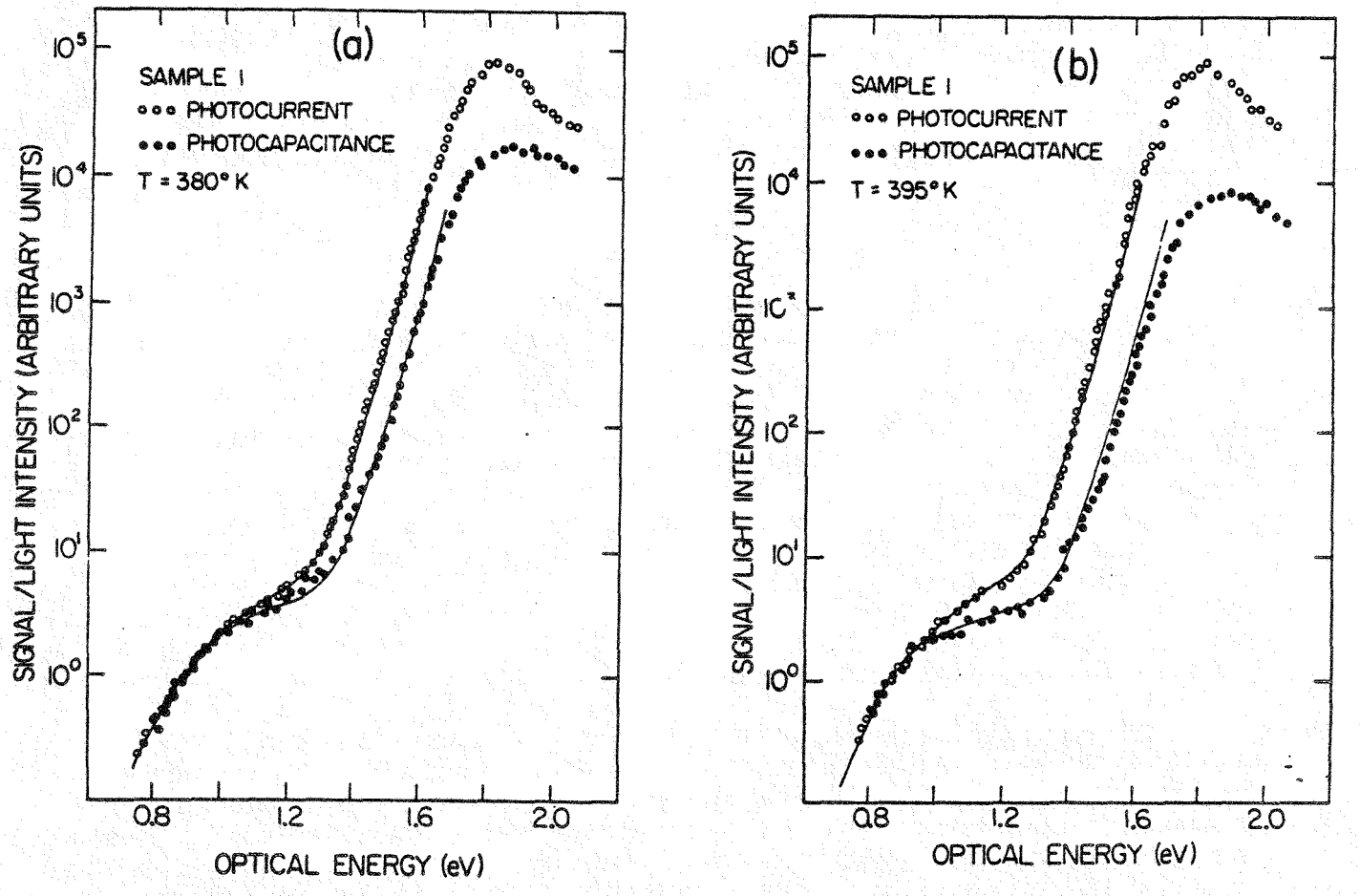

FIG. 4. Comparison of transient photocapacitance and transient junction photocurrent spectra for (a) 380 K, and (b) 395 K. The two kinds of spectra have been overlapped in the low optical energy regime in each case. The thin solid lines indicate the results of model calculations obtained using Model I in Fig. 5.

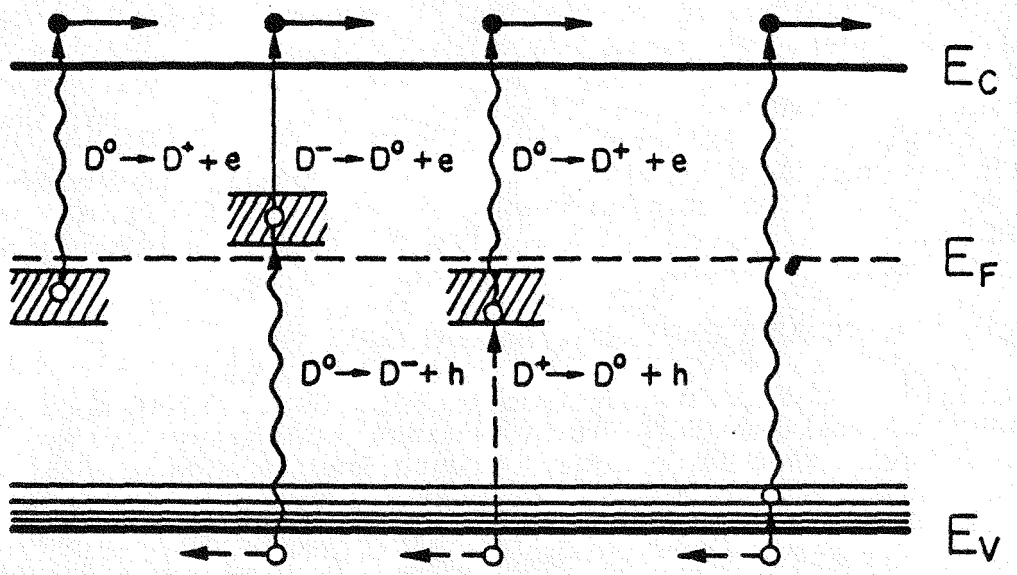

MODEL I

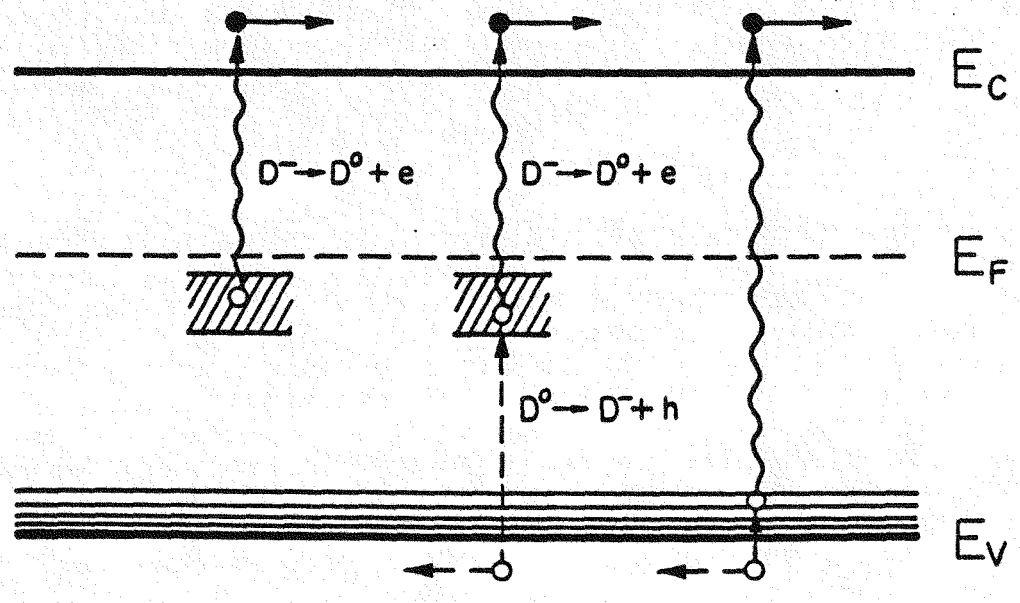

MODEL II

FIG. 5. Schematic of two deep defect models used to fit the spectra of Fig. 4. Possible optical transitions are indicated by wavy lines, fast thermal transitions are indicated by solid vertical lines, and slower thermal transitions are indicated by dashed vertical lines. Horizontal arrows indicate electron and hole transport out of the depletion region with dashed lines indicating that holes will be partially retrapped before escape.

Applying this reasoning we may thus determine from the ratios of the photocurrent to the photocapacitance at 1.6 eV for this sample that 67% of the trapped holes are swept out of the depletion region at 380K while 84% escape at 395K (the measurement timescale for these spectra was 4 seconds). In general, all differences between the photocapacitance and photocurrent spectra displayed in Fig. 4 are attributable to hole emission and/or transport processes. We see that these processes have an onset energy of about 0.95 eV for this sample and that they are strongly temperature dependent.

5.2 MODELING OF THE EXPERIMENTAL SPECTRA

Following the discussion above, the successful modelling of such experimental spectra will require the incorporation of the optical transitions of electrons into and out of defect states, the thermal emission of gap state electrons and holes to the conduction and valence bands, respectively, plus an assessment of the ability of a valence band hole to escape the depletion region.

First, let us discuss the effects of the limited hole mobility in analyzing our spectra. (We will assume that, due to their much higher mobility, that electrons emitted optically or thermally to the conduction band will always escape on our experimental time scale.) All transitions of electrons from the VB-tail leave holes which are thermally emitted very rapidly to the valence band mobility edge. However, before these holes can be swept out of the depletion region, a significant fraction will be trapped at deep localized states. The average distance $L_d(x)$ which the thermally emitted hole will travel before it gets trapped is

$$L_d(x) = (\mu\tau)_h \, E(x) \qquad (5)$$

where x is the distance of the photoexcited hole measured from the junction interface and E(x) is the electric field at x. Note that Eq. (5) is an approximation in that it assumes that each hole travels under a constant electric field during t_h and is thus strictly valid only in the low mobility limit. A thermally emitted hole can escape from the depletion region only if $L_d(x) > x$. Because an increase of temperature will generally increase both E(x) (due to fewer trapped electrons) as well as $(\mu\tau)_h$, the number of holes which can escape will be increased. Consequently, the valence bandtail photocapacitance signal will decrease relative to the photocurrent signal as observed.

Next, we must consider the possible transitions from deep states. A schematic representation of these kinds of transitions is given in Fig. 5. Here we display two possible models for deep states in undoped a-Si:H. In both models we have assumed that the only defect in the gap is a "dangling bond" (D) with a positive correlation energy. We employ a Gaussian shaped defect band of D gap states whose absolute magnitude is derived from

drive-level measurements, and whose energy position and width are estimated by directly fitting the shapes of the transient photocurrent and photocapacitance spectra as described below. The Fermi level position is determined from capacitance vs. temperature and drive level measurements.

In model I we assume that the charge state of the dangling bond defect is neutral (D^o) in equilibrium. We therefore consider the optical deep defect transitions $D^o \longrightarrow D^+ + e$, plus $D^o \longrightarrow D^- + h$ together with the thermal transition $D^+ \longrightarrow D^o + h$. The thermal emission rate is an adjustable parameter. Since the position of the D^- band lies above the Fermi level, the optical transition $D^o \longrightarrow D^- + h$ is always followed by the thermal transition $D^- \longrightarrow D^o + e$ with an emission time much shorter than our measurement time. The optical transition $D^o \longrightarrow D^- + h$ therefore primarily enhances the transient photocurrent signal and contributes to the transient photocapacitance at a significantly reduced level.

In model II the charge state of the dangling bond defect in equilibrium is assumed to be negative (D^-). Thus in this case we consider the optical transition $D^- \longrightarrow D^o + e$, and the thermal transition $D^o \longrightarrow D^- + h$ again with an adjustable thermal emission rate. Note that there is no transition in model II similar to the optical transition $D^o \longrightarrow D^- + h$ of model I. Finally, for both models we assume that the photoexcited hole for valence band optical transitions is thermally emitted to the valence band very fast compared to the measurement time scale so that the transient photocapacitance signal observed for such transitions depends only on $L_d(x)$.

The exponentially increasing portions of both the photocurrent and photocapacitance spectra (the valence bandtail region of g(E)) yield the same characteristic energy, E_o, within the experimental uncertainty ($E_o = 42 \pm 2$ meV). From the difference in magnitude between photocurrent and photocapacitance in this energy range we find a $(\mu\tau)_h N_T$ value for holes equal to 4.8×10^6 cm^{-1} V^{-1} at 380K and 7.0×10^6 cm^{-1} V^{-1} at 395K. Here N_T is the total density of D defects as determined from drive-level measurements [8]. These values are in good agreement with earlier studies[12] and indicate a weakly temperature dependent hole capture process.

The energy regime of the spectra below 1.5 eV are attributed to optical electron and hole transitions on dangling bond defects. We extract the component that corresponds to electron transitions (see earlier discussion) and deconvolve this signal assuming a square root energy dependence of the conduction band density of states for $E > E_c$ and a single Gaussian deep defect band. A best fit places its energy position at 0.95 eV below E_c with a sigma (energy width) of 0.14 eV and a magnitude of 1.1×10^{16} cm^{-3} eV^{-1}.

We identify the difference between photocurrent and photocapacitance in the energy range between 1.1 and 1.5 eV as due to the thermal transition $D^+ \longrightarrow D^o + h$ (in model I) or $D^o \longrightarrow D^- + h$ (in model II). In these cases the hole thermal emission rate depends on the energy difference, as measured from the valence band mobility edge, of the hole left behind by the optical transition $D^o \longrightarrow D^+ + e$ in model I, or $D^- \longrightarrow D^o + e$ in model II, respectively (see Fig. 5). Thus a photoexcited hole which is left closer to the valence band will be thermally emitted much faster than a photoexcited hole which lies closer to the middle of the gap. This simple principle naturally accounts for the observed strong temperature dependence of the deviation between the photocurrent and photocapacitance spectra as displayed Figs. 4a and 4b. We thus determine that the thermal emission rate prefactor the deep hole emission in either model is 10^{12} sec^{-1} assuming a thermal gap $E_g^{th} = 2.0$ eV at 380K. This gap value is larger by 0.3 eV than the optical gap, E_g^{opt}, which we determine be 1.67 eV at this temperature. The value of E_g^{opt} is obtained in our analysis from the energy difference between the conduction and valence bands at the density of states value of 10^{21} cm^{-3} eV^{-1}. (A more traditional "Tauc" optical is likely to be larger [13].) Note that the value of E_g^{th} determined here is very close to the thermal gap values determined from DLTS [14].

We display final fits based on model I in Fig. 4 (solid lines). This model does, in fact, offer a somewhat better fit than is possible using model II. On the other hand, we note that the energy of 0.95 $\pm$ 0.03 eV determined for this undoped sample for the electronic optical transition from the defect is very close to the average value of E_c - 0.92 eV for the dominant deep defect which we have determined in our studies of n-type doped films[9]. In that case we can unambiguously identify that defect transition as $D^- \longrightarrow D^o + e$ [15]. An alternative argument for nonetheless identifying the midgap transition in undoped a-Si:H to D^o/D^+ has been proposed by Kocka et. al.[16].

5.3 STUDIES OF METASTABLE EFFECTS

In Fig. 6 we display transient photocurrent and photocapacitance spectra for sample 4 in the fully dark annealed state (state A) and a metastable state reached by annealing at 410K for 15 minutes following light soaking. We observe an increase of the defects in the partially annealed state by a factor of 3.3 compared to state A, in agreement with our earlier studies[8]. We analyze these spectra as before; we find the energy position and width of the defect optical transition are E_c - 0.94 eV and 0.13 eV, respectively, with a magnitude of 1.6×10^{16} cm^{-3} eV^{-1} in state A and 5.25×10^{16} cm^{-3} eV^{-1} in the partially annealed light-soaked state. The optical gap value at 380K is 1.78 eV. For $(\mu\tau)_h N_T$ we obtain 4.35×10^6 cm^{-1} eV^{-1} $\pm$ 20% in state A and 1.705×10^6 cm^{-1} eV^{-1} $\pm$ 20% in the partially annealed state. The difference in the two values

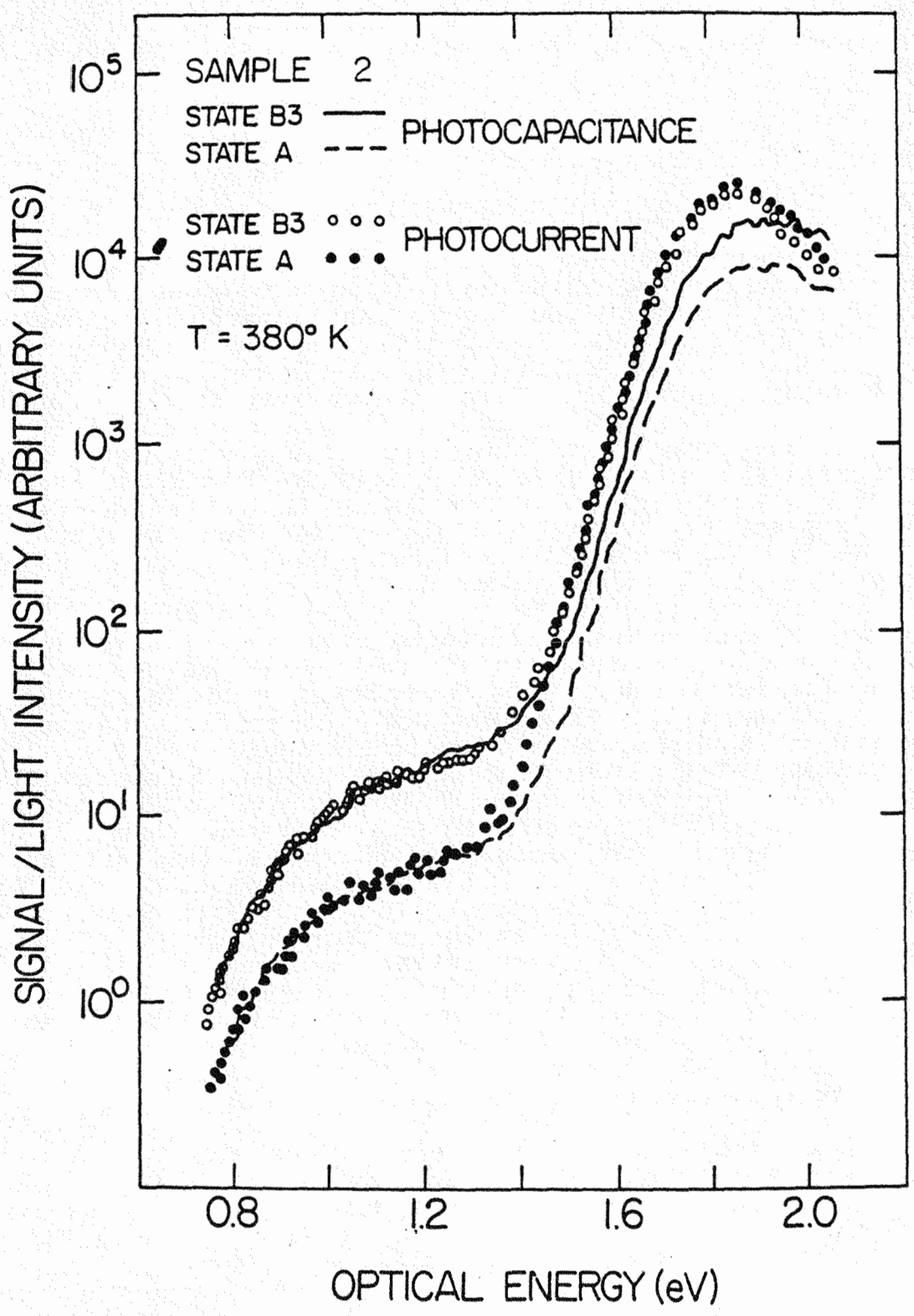

FIG. 6. Comparison of transient photocapacitance and photocurrent spectra for Sample 2 before and after light soaking.

indicates that $(\mu\tau)_h$ decreases as we approach the fully light soaked state. The most plausible explanation for such a result is that the light-induced metastable defects have a larger capture cross-section (by a factor of 3.3) than the intrinsic defects.

6.0 STUDIES OF METASTABLE EFFECTS IN N-TYPE DOPED FILMS

6.1 DRIVE-LEVEL STUDIES OF METASTABLE EFFECTS

In Fig. 7 we present drive-level profiles, N_{DL}, for a series of measurements for the last several anneals of a sequence of metastable states between the light soaked state B and state A. As explained in Section 3.1, each of these curves represents a spatially averaged integral over g(E) as a function of (thermal) energy below the neutral bulk Fermi energy (see Eq. 2). For each of these metastable states E_F^o is well within the conduction band tail. The relatively flat dependence of N_{DL} between 200K and 300K indicates that g(E) has a relatively low magnitude over the energy range between 0.3 and 0.6 eV below E_c. Thus we may take the value N_{DL} at, say, 240K (E_e = 0.4 eV) as representative the occupied density of conduction bandtail states, N_{BT}, for each of the metastable states in this sample.

We may determine the approximate position of E_F^o for each metastable state from the activation energy of conductivity which, as described previously, we obtain quite reliably for these sandwich geometry samples from capacitance-temperature measurements at a series of measurement frequencies [14]. Thus we plot in Fig. 8 the number of occupied bandtail states relative to state A, N_{BT}, *vs.* the bulk Fermi level position for the final sequence of anneals for each of our 3 doped samples. As expected, the density of occupied conduction bandtail states increases as E_F^o moves to shallower energies. The only exceptions sometime occur for the final high temperature state A anneal (see behavior for samples 2n and 3n in Fig. 8). However, because the 473K annealing temperature employed for this final anneal occurs above the re-equilibration temperature at which defect energies may be redistributed [17], this sort of anomaly is not entirely unexpected. Rather, we wish to focus on the fact that N_{BT} increases significantly for each of the anneals for all samples up to the final anneal employed.

At higher temperatures the drive level profiles give us information about the distribution of the deeper states. However, except as an aid for setting the absolute magnitude of g(E) in this region, we prefer to obtain the deep defect densities from the photocapacitance spectra discussed in the next section. Those data not only give g(E) over a wider energy range but are also free of anomalies such as quasi-Fermi level cutoffs and "area spreading" [18] which often make these drive-level spectra difficult to interpret at higher temperatures for such relatively high conductivity samples.

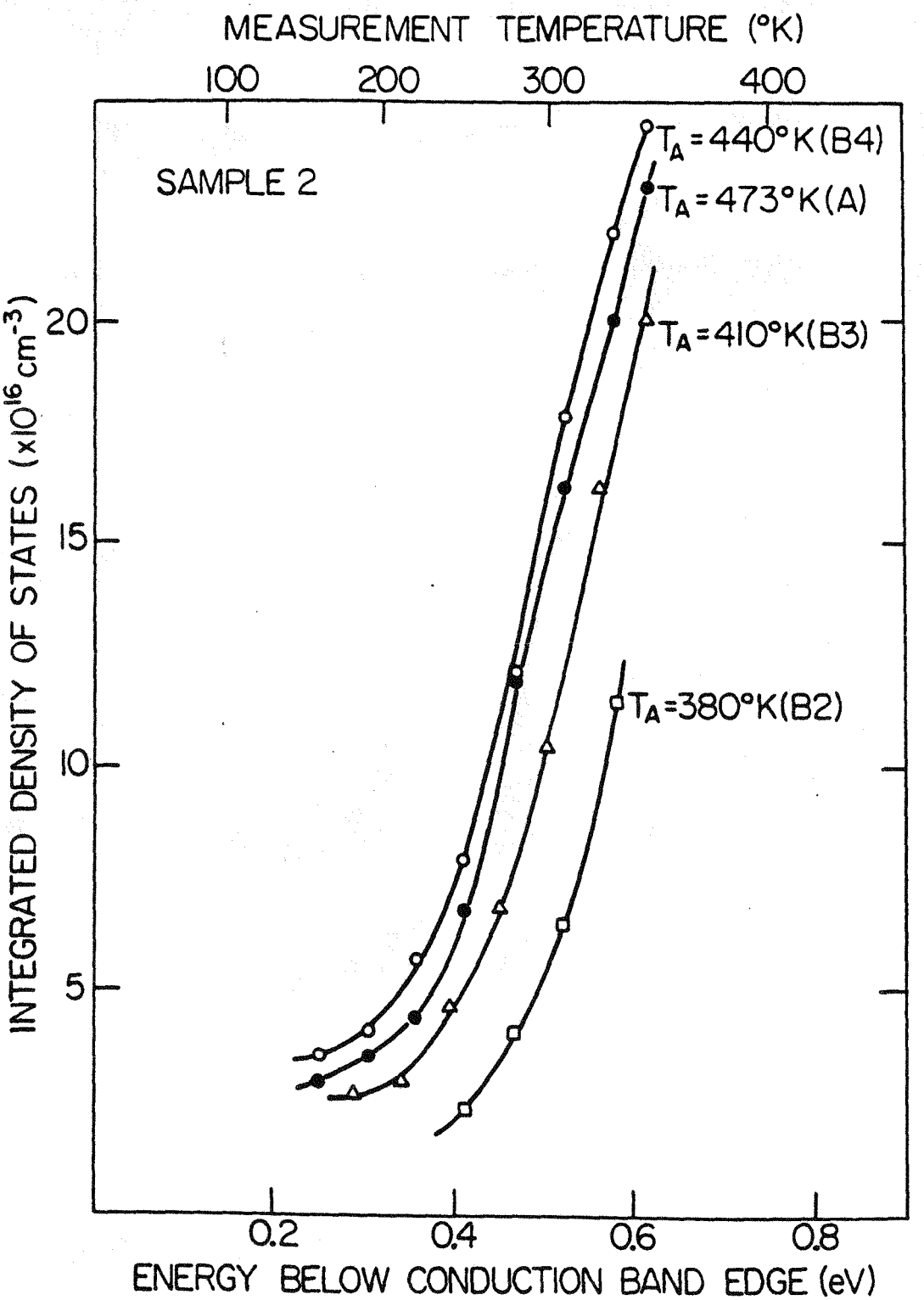

FIG. 7. Drive-level densities vs. temperature (energy below E_c) for the 100 vppm PH_3 doped sample for state A and 3 partially annealed light-soaked states between state B and state A. The low temperature limiting value of these curves gives the density of occupied bandtail states, N_{BT}.

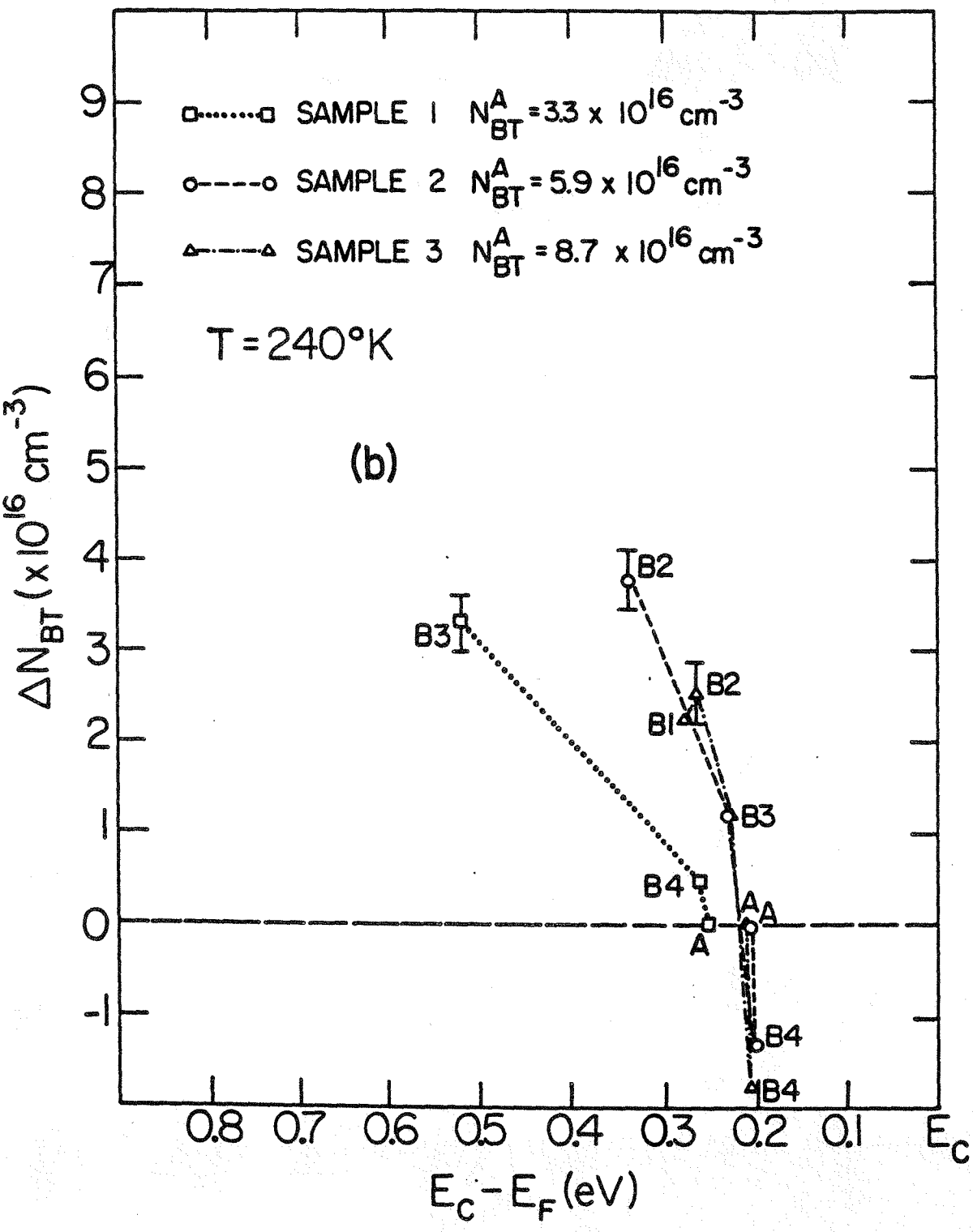

FIG. 8. Variation in the density of occupied bandtail states, ΔN_{BT}, with Fermi level position for sequences of partially annealed metastable states for three n-type samples of 30 vppm PH_3 (sample 1), 100 vppm PH_3 (sample 2), and 300 vppm PH_3 (sample 3) doping levels. Bandtail occupation densities are given relative to those in state A for each sample (dashed horizontal line) and state A values of N_{BT} are listed at the top of the figure.

6.2 TRANSIENT PHOTOCAPACITANCE STUDIES

Transient photocapacitance spectra for the 30 vppm PH_3 doped sample are displayed in Fig. 9 for state A, state B1 (380K anneal), and state B2 (410K anneal). To compare these spectra we have overlapped them in the VB-tail region as is customary. These spectra indeed indicate significant changes in the deep defect region of the spectra as this samples is annealed. First, in the anneal between states B1 and B2 the dangling bond signal decreases by an amount which is independent of the optical energy, thus indicating a decrease of the density but not the energy distribution of the midgap defect level. However, in the anneal to state A, the shape of the photocapacitance spectrum in the defect region also changes significantly and indicates the part of the defect near midgap anneals faster than that near the valence bandtail. Similar but less pronounced asymmetries are also observed for the 100 vppm PH_3 sample, while for the most heavily doped sample there is no such detectable behavior.

Similarly to Fig. 8, in Fig. 10 we plot the change in density of dangling bond defects, N_D, for the full sequence of partial anneals for each sample vs. the position of the bulk Fermi energy. This has been accomplished by choosing the value of the photocapacitance signal at 1.2 eV which is essentially proportional to the integral over the deep states between E_c - 0.6 eV and E_c - 1.2 eV. The absolute magnitudes of the deep defect densities are obtained by calibrating them against the drive-level profiles at higher temperatures. As would be expected, this defect density is observed to decrease monotonically as the sample is annealed. However, we observe that it decreases significantly only for the earlier anneals and then remains essentially constant for anneals higher than 430K. This is to be contrasted with the annealing behavior of the occupied bandtail states displayed in Fig. 8 which shows a significant changes up to the highest anneal temperatures.

6.3 DISCUSSION OF RESULTS

We shall discuss the above results on n-type doped films in terms of various possible metastable defect models which have been proposed over recent years. In the case of undoped a-Si:H samples, the most popular model explains the observed behavior by proposing that the recombination of photoinduced carriers breaks weak Si-Si bonds and creates dangling bonds [1,2]. For n-type doped films, due to the presence of the conduction bandtail electrons, this reaction becomes:

$$2e^- + 2Si_4^o \longrightarrow 2Si_3^- \qquad \text{(i)}$$

Here Si_3^- represents a negatively charged dangling bond and Si_4^o represents a 4-fold coordinated Si atom in its bonding state. The experimental signature of this reaction would be a shift of

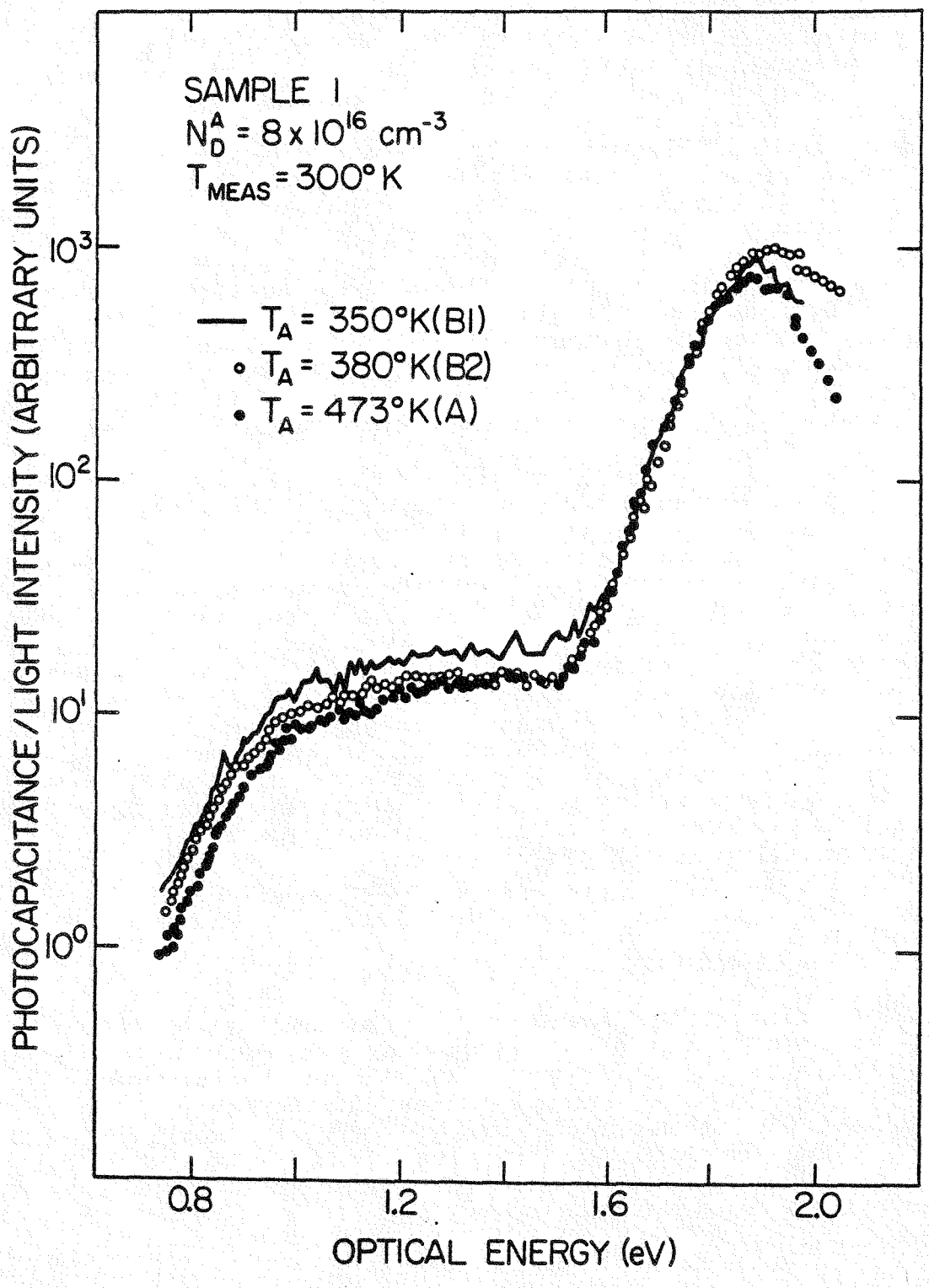

FIG. 9. Photocapacitance spectra vs. optical energy for the 30 vppm PH_3 samples in state A and two partially annealed light-soaked states. Spectra are overlapped in the valence bandtail region.

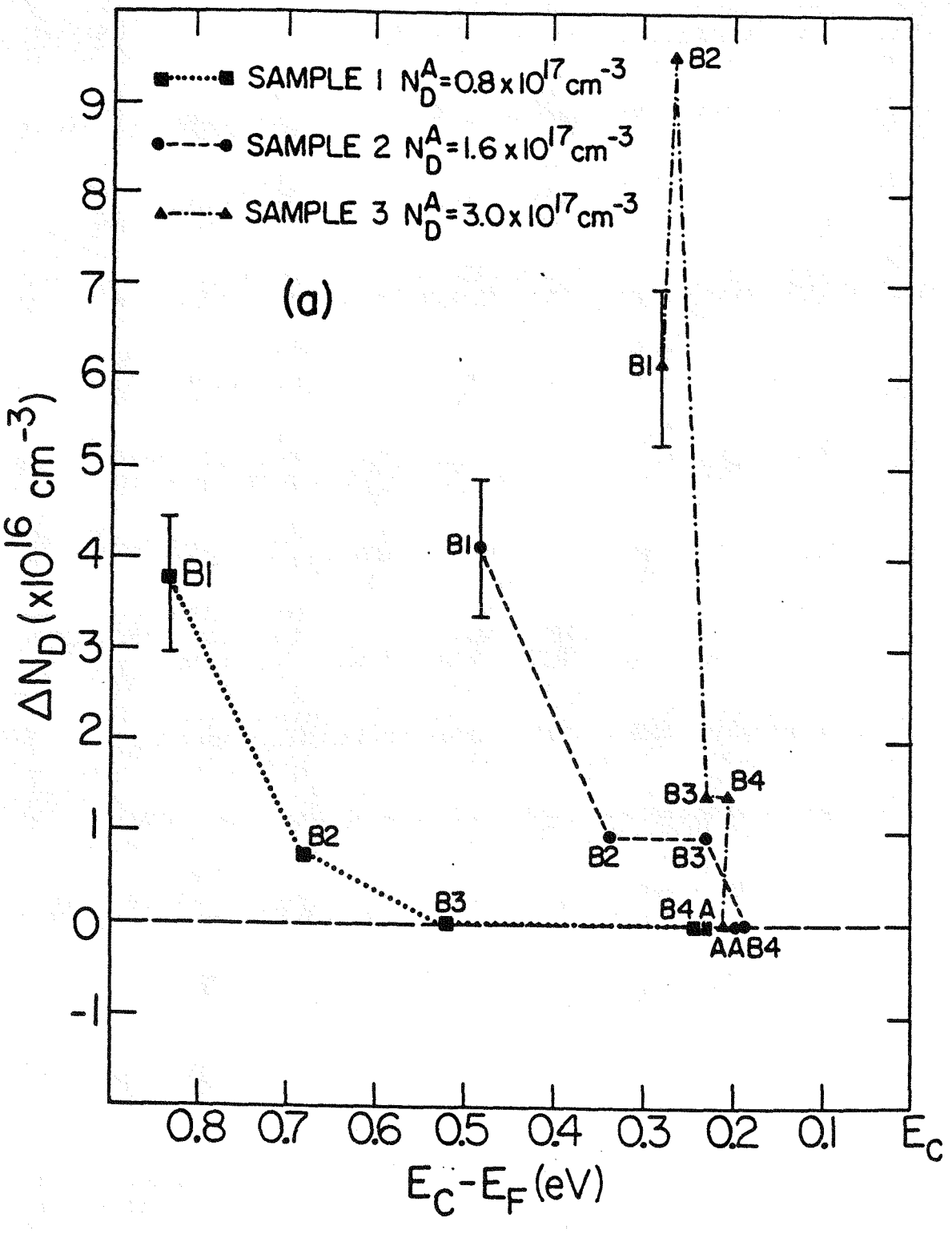

FIG. 10. Variation in the density of deep defect states, ΔN_D, with Fermi level position for sequences of partially annealed metastable states for three n-type samples. Deep defect densities are given relative to those in state A for each sample and those state A values are listed at the top of the figure.

E_F, with a concomitant change in N_{BT}, in direct proportion to the change in N_D.

Additional reaction involve dopant atoms directly. Two reactions which have been suggested are:

$$Si_4^o + P_3^o \longrightarrow Si_3^o + P_4^+ \qquad \text{(ii)}$$

$$Si_3^- + P_3^o \longrightarrow Si_4^- + P_4^o \qquad \text{(iii)}$$

both of which require either the annihilation or the creation of a dangling bond defect [8,19]. In these latter two reactions P_3 represents a phosphorous atom in a non-doping configuration and P_4 represents a phosphorous atom in a doping configuration.

The likely signature of reaction (ii) would be an observed change in N_D with little or no shift in E_F (E_F would remain pinned between the D^- and P_4^+ defect bands). Reaction (iii) would, like reaction (i), cause a change in bandtail occupation equal to the corresponding change of N_D (in this case these conduction bandtail states include the P_4 donor band).

Our experimental results as presented in Figs. 8 and 10 give us the kind of detailed information by which we should be able to identify which of the above defect reactions is dominant. We observe that as we approach state A the general trend in all three samples is, indeed, the decrease of the photoinduced D^- states and the increase of the occupied bandtail states. Note that we can shift E_F to energies deeper than 0.8 eV below E_c in the lightly doped film, but that this E_F shift decreases with doping. We also note that the number of photoinduced D^- states also appear to scale with the doping level as previously observed [20]. Most importantly, we observe that in the lowest doped sample the light induced changes of the D^- states annealed at significantly lower temperatures than the changes in the bandtail occupation. This effect is less pronounced for sample 2 and non-existent for sample 3. This behavior <u>cannot</u> be explained by any of the three reactions given above. Although reaction (i) can explain the E_F shift, it also requires a correlation between changes in bandtail and D^- states. Reaction (ii) cannot explain the E_F motion and the increase in the bandtail signal, while reaction (iii) again predicts photoinduced changes completely opposite from the ones observed. If a combination of (i) and (ii) were at work [19] then we would expect an increase of the bandtail signal and an even stronger decrease in the D^- signal as state A is approached, which is not observed.

Thus we infer the existence of a defect reaction in the lower doped film which can change the doping configuration of phosphorous independent of changes in the D^- density. This conclusion is similar to that previously drawn by DLTS studies [18]. As the doping level is increased, we might well expect reaction (ii) to become dominant. In such a case we should see a small E_F shift, a N_D signal decreasing with anneal temperature

and small changes in the bandtail state occupation. Sample 3 appears to indeed exhibit such a behavior.

Our results therefore strongly suggest that different reactions are dominating the photoinduced changes at different phosphorous doping levels. We wish to stress that these conclusions are obtained only because we have carefully monitored the changes in both the D^- and the occupied bandtail states for a sequence of metastable states from full light saturation to state A. We know of no other study which has investigated metastable behavior in n-type a-Si:H in this manner of detail.

7.0 GENERAL DISCUSSION

7.1 SUMMARY OF RESULTS OBTAINED

In this Subcontract period, as described above, we have developed and exploited 2 types of junction capacitance methods for the study of metastable effects in a-Si:H films. First of all, we have continued our investigation of light-induced effects in undoped samples using the drive-level capacitance profiling method. In addition to extending these studies to two new "totally phosphorous free" samples, we also began to better exploit the profiling aspect of this technique by comparing the spatial dependence of the metastable deep state distribution with the SIMS determined impurity profiles for these samples. Such studies appear to confirm our earlier conclusions that there exists a strong correlation between the impurity content in a-Si:H films with the degree of the light-induced defect creation, particularly in the case of carbon impurities.

Second, we developed the method of transient photocapacitance spectroscopy to the study of undoped films. We found that, by comparing such spectra to junction transient photocurrent spectra taken under identical conditions, we could unambiguously separate the electron and emission transition from deep gap states. Our analysis also allowed us to determine the hole $\mu\tau$ products. Moreover, by comparing films before and after light soaking we found that the $(\mu\tau)_h$ product was larger for the light-induced defects than for the intrinsic defects, by roughly a factor of 3.

Finally, we applied both the drive-level capacitance profiling method and the transient photocapacitance method to the study of metastable effects in n-type doped samples. These studies were intended to help identify which of various proposed defect reactions might be responsible for the observed changes with regard to Fermi level position, occupied bandtail states, and density of deep "dangling bond" defects. Our results indicated that none of the suggested reaction could explain the behavior of the most lightly doped samples and indicated, instead, that there exists a reaction involving dopant vs. non-doping configurations of P by itself. On the other hand, in the

more heavily doped (300 vppm PH_3) samples, the behavior seemed to indicate a dominant role for the reaction $Si_4^o + P_3^o \longrightarrow Si_3^o + P_4^+$.

7.2 FUTURE RESEARCH DIRECTIONS

The results obtained during this Subcontract period raise significant questions regarding mechanisms for light-induced defect creation in a-Si:H. Many of these are important areas for further research. First of all, the compelling evidence for a strong extrinsic component in the instability in undoped films needs to examined further to establish the minimum atmospheric impurity levels which can affect stability.

Second, it would be quite valuable to try to establish a correlation between growth method (photo-CVD, H_2 dilution during growth, etc.) and the degree of stability in a-Si:H films. The two techniques we have described above, drive-level capacitance profiling and transient photocapacitance would be quite well suited to this purpose since they seem to give a quite complete picture of the kinds of changes that are taking place.

Third, similar sorts of studies should be carried out on amorphous semiconductor alloy films. The development of amorphous silicon/germanium alloys has been very important in efforts to fabricate tandem solar cells to improve solar cell efficiencies. Beginning with fairly dilute Ge alloys, one could carry out the same kinds of studies as with the pure a-Si:H films to discern whether there are particular kinds of instability effects peculiar to this alloy system. Depending on the ability to fabricate good diode barrier junctions on these materials, such studies could hopefully be used to investigate the full alloy system.

Finally, the fundamental issues concerning the microscopic mechanisms of metastable effects in a-Si:H are still not well resolved. Of particular interest would be to extend many of the above kinds of studies to other kinds of metastable states of this material, including those obtained by quench cooling [17] and bias annealing [21]. Because all of these effects do, indeed, seem to be related, some very valuable insight is likely to be obtained by such comparisons. Although a substantial amount of evidence has now been obtained implicating hydrogen motion in these effects [22], alternative models continue to be proposed which seem to explain some aspects of these metastable behaviors. Clear experimental evidence to distinguish between these possible models must continue to be sought. We believe, that our junction capacitance based studies have an excellent chance to give a more complete picture of what lies behind these effects.

8.0 REFERENCES

1. H. Dersch, J. Stuke, and J. Beichler, J. Phys. Status Solidi(b), 105, (1981) 265.

2. M. Stutzmann, W.B. Jackson, and C.C. Tsai, Phys. Rev. B, 32, 23 (1985).

3. O. Stika and A. Triska, Solar Energy Materials 8, 411 (1983).

4. C.R. Wronski, Z E. Smith, S. Aljishi, V. Chu, K. Shepard, D.S. Shen, R. Schwarz, D. Slobodin, and S. Wagner, in Stability Issues in Amorphous Silicon Alloys, ed. by B. Stafford and E. Sabisky, (AIP Conf. Proc., New York, 1987), Vol. 157, p. 20.

5. N.M. Amer and W.B. Jackson, in Semiconductors and Semimetals, ed. by J. Pankove (Academic Press, New York, 1984), Vol. 21B, p. 83.

6. SIMS analysis for C,N, and O impurities for samples 1-6 and P content for all samples performed by Charles Evans and Associates, Redwood City, California. C,N, and O analysis on samples 7 and 8 was carried out at SERI, Golden, Colorado.

7. C. E. Michelson, A. V. Gelatos, and J. D. Cohen, Appl. Phys. Lett. 47, 412 (1985).

8. K.K. Mahavadi, K. Zellama, J.D. Cohen, and J.P Harbison, Phys. Rev. B35, 7776 (1987).

9. A.V. Gelatos, J.D. Cohen, and J.P. Harbison, Appl. Phys. Lett., 49, 722 (1986).

10. See, for example, D.E. Carlson, J. Vac. Science and Tech. 20, (1982).

11. D.V. Lang in Topics in Applied Physics, ed. by P. Braunlich (Springer, Berlin, 1979), Vol. 37, p. 93.

12. R.A. Street, J. Zersh, and M.J. Thompson, Appl. Phys. Lett. 43, 672 (1983).

13. W.B. Jackson, S.M. Kelso, C.C. Tsai, J.W. Allen, and S-J. Oh, Phys. Rev. B 31, 5187 (1985).

14. D.V. Lang, J.D. Cohen, and J.P. Harbison, Phys. Rev. B25, 5285 (1982).

15. J.D. Cohen, J.P. Harbison, and K.W. Wecht, Phys. Rev. Lett. 48, 109 (1982).

16. J. Kocka, J. Non-Cryst. Solids 90, 91 (1987).

17. J. Kakalios and R.A. Street, Phys. Rev. B 34, 6014 (1986).

18. D.V. Lang, J.D. Cohen, J.P. Harbison, and A.M. Sergent, Appl. Phys. Lett. 40, 474 (1982).

19. M. Stutzmann, Phys. Rev. B 35, 9735 (1987).

20. A. Skumanich, N.M. Amer, and W.B. Jackson, Phys. Rev. B 31, 2263 (1985).

21. D.V. Lang, J.D. Cohen, and J.P. Harbison, Phys. Rev. Lett. 48, 412 (1982).

22. For one recent account see W.B. Jackson and D.M. Meyer, Proc. Mat. Res. Soc., (1988 Spring Meeting, Reno), to be published.

9.0 PERSONNEL AND ACKNOWLEDGEMENTS

J. David Cohen	Principal Investigator/Program Manager
Krishna Mahavadi	Research Associate -- Phase I
Jerry Gelatos	Research Associate -- Phase II
John Essick	Research Assistant/Graduate Student

ACKNOWLEDGEMENTS

We would like to thank James P. Harbison of Bell Communications Research, Inc., for providing many of the samples used in these studies. We also gratefully acknowledge the generous equipment gifts of Tektronix, Inc., during each of the 2 phases of this SERI Subcontract which contributed greatly to the success of this research program.

Document Control Page	1. SERI Report No. SERI/STR-211-3448	2. NTIS Accession No. DE89000890	3. Recipient's Accession No.

4. Title and Subtitle

Investigations of the Origins of Metastable, Light-Induced Changes in Hydrogenated Amorphous Silicon
Final Subcontract Report, 1 Feb. 1986-30 Mar. 1988

5. Publication Date: March 1989

6.

7. Author(s)
J. David Cohen

8. Performing Organization Rept. No.

9. Performing Organization Name and Address

Department of Physics
University of Oregon
Eugene, Oregon 97403

10. Project/Task/Work Unit No.

11. Contract (C) or Grant (G) No.
(C) XB-6-06024-1
(G)

12. Sponsoring Organization Name and Address

Solar Energy Research Institute
1617 Cole Boulevard
Golden, Colorado 80401-3393

13. Type of Report & Period Covered
Technical Report

14.

15. Supplementary Notes
SERI Technical Monitor: Byron Stafford, (303) 231-7126

16. Abstract (Limit: 200 words)

This report contains results of Phase II of research to investigate metastable defect creation processes in hydrogenated amorphous silicon. The study relied primarily on junction capacitance methods to monitor the changes in deep defect distribution. Results obtained applying capacitance profiling methods to the study of undoped samples are summarized and indicate a significant role of extrinsic impurities in the degree of light-induced degradation that occurred. Photocapacitance transient measurements were taken to investigate changes in undoped a-Si:H. Studies were also begun of metastable changes in n-type doped a-Si:H samples by using both the drive-level capacitance profiling technique and transient photocapacitance methods, and results are described.

17. Document Analysis

a. Descriptors
Amorphous state ; silicon solar cells ; metastable states ; energy losses

b. Identifiers/Open-Ended Terms

c. UC Categories
271

18. Availability Statement

National Technical Information Service
U.S. Department of Commerce
5285 Port Royal Road
Springfield, Virginia 22161

19. No. of Pages
36

20. Price
A03